Applied Geochemistry 127 (2021) 104908

Contents lists available at ScienceDirect

Applied Geochemistry

journal homepage: http://www.elsevier.com/locate/apgeochem

Anthropogenic gadolinium in estuaries and tropical Atlantic coastal waters from Fortaleza, Northeast Brazil

Antonia Rute B. da Costa [a], Tristan C.C. Rousseau [a,*], Poliana D. Maia [b], Artur M. Amorim [c], Fernando F. Sodré [c], Carlos Eduardo P. Teixeira [a]

[a] Instituto de Ciências Do Mar, Universidade Federal Do Ceará, Fortaleza, CE, CEP 60165-081, Brazil
[b] Faculdade de Planaltina, Universidade de Brasília, Área Universitária N.1, Vila Nossa Senhora de Fátima, Planaltina, 73300-000, Brazil
[c] Instituto de Química, Universidade de Brasília, Brasília, DF, CEP 70297-400, Brazil

ARTICLE INFO

Editorial handling by Dr. Z Zimeng Wang

Keywords:
Rare earth elements
Anthropogenic Gd
Emerging contaminant
Sewage outfall
Coastal waters
Source tracer

ABSTRACT

Gadolinium-based contrast agents are worldly used for medical magnetic resonance imaging and are an emerging contaminant in natural waters. We investigated the dissolved fraction of Gd in coastal waters from Fortaleza city and observe positive Gd anomalies in the wastewater outfall area as well as in two local river estuaries indicating that the city is a significant source of anthropogenic Gd (Gd_{anth}) to the ocean. Based on this synoptic study and on the conservative behavior of Gd_{anth} we trace a highly concentrated sewage-based source which accounts for 2200 pmol kg^{-1} and to an annual discharge of 25 kg of Gd to the ocean. We also trace minor sources from the two rivers and estimate that the levels of wastewater dilution within freshwater prior to mixing with seawater accounted for 4.8%–14% of the Cocó River discharge and 1.4%–3.9% of the Ceará River discharge at the time of the sampling. Gd is consequently a suitable and promising tracer for water management and forensic purposes in Fortaleza. In order to guide the application of this method to other coastal waters impacted by metropolitan areas in the world, we propose a conceptual model for Gd_{anth} behavior within salinity gradients and apply it to revisit previous studies.

1. Introduction

Rare earth elements (REE) form a group of elements of similar physical-chemical properties due to the gradual filling of their 4f electronic shell. Their increase in atomic number is associated with a decrease in ionic radii (Henderson 1984) leading to coherent behavior with subtle variations in reactivity and relative abundance (Sholkovitz et al. 1994; Coppin et al., 2002; Luo and Byrne 2004; Köhler et al., 2005), being therefore suitable geochemical tracers of sources and processes for rocks and aqueous media. In contrast with strictly trivalent REE, cerium and europium exist in tetravalent and bivalent state respectively. Thus, they can fractionate substantially compared to their neighbors forming a naturally occurring anomaly (Elderfield 1988).

Anomalous gadolinium concentrations were first observed in samples from the Rhine River (Bau and Dulski 1996) and have since been reported in several aquatic environments located in densely populated areas around the world (Nozaki et al., 2000; Bau et al., 2006; Lawrence 2010; Hatje et al., 2016; Mortatti and Enzweiler 2019). Such anomalies can reach several orders of magnitude higher than the background Gd concentrations and are linked to anthropogenic sources related to medical activities. Gd-based contrast agents (Gd-CAs) are extensively used for magnetic resonance imaging (MRI) exams since their first approval in 1988 (Zhou and Lu 2013). As free Gd^{3+} in the bloodstream is toxic, Gd-CAs consist of chelate molecules resistant to rupture by metabolic processes and being rapidly eliminated through renal excretion (Oksendal and Hals 1993; Kümmerer and Helmers 2000; Pałasz and Czekaj 2000; Shellock 2000; Feng et al., 2010; Xia et al., 2011). Natural levels of Gd in several water bodies, used as wastewater receptors, have been exceeded (Möller et al., 2000) leading, in some regions, to contamination of soils and adjacent aquifers used as drinking water sources (Schmidt et al., 2019).

This exceeding Gd behaves conservatively and is rarely removed in wastewater treatment plants (Rabiet et al., 2014). This behavior is ascribed to the fact that Gd ligands have a high complexation capacity with Gd and shall be non-reactive with surfaces and suspended sediments, refractory to pH variation range of different media (blood,

* Corresponding author.
E-mail address: tristanrousseau@ufc.br (T.C.C. Rousseau).

https://doi.org/10.1016/j.apgeochem.2021.104908
Received 24 November 2020; Received in revised form 10 February 2021; Accepted 10 February 2021
Available online 16 February 2021

continental water and seawater) and to bacterial activity (Schijf and Christy 2018). The conservative behavior of Gd complexes allows to trace pollution sources associated with treated and untreated wastewaters and levels of Gd may depend on population density, the numbers of MRI exams which are growing worldwide and wastewaters dilution by natural waters (Möller et al., 2000; Bau et al., 2006; Kulaksız and Bau 2007; Lerat-Hardy et al., 2019). This behavior contrasts with natural Gd and other REE which are highly reactive and tend to associate with organic and mineral colloidal ligands removed from the water column in estuaries (Sholkovitz 1993; Rousseau et al., 2015). To date, the toxicity of this emerging contaminant and its long-term lability are still poorly known (Henriques et al., 2019; Fujita et al., 2020) and its levels have shown a significant increase over short periods of time in some locations (Tepe et al., 2014; Hatje et al., 2016).

In a recent study, Pedreira et al. (2018) observed the presence of Gd anomalies in coastal waters near the outfalls of two WWTP from Salvador city, northeast Brazil. The authors measured the anthropogenic Gd concentration within these WWTPs and used national wastewaters discharges data to perform a mass balance of its load exported annually by Brazilian coastal cities outfalls. The present work was developed in Fortaleza city, the capital of Ceará state located in the northeast region of the country (Fig. 1). Fortaleza is the fifth Brazilian city in population size and has 35 magnetic resonance facilities, i.e., 1.3 equipment per 100,000 inhabitants (Datasus, 2019), which is close to the 1.6 average ratio observed for the Organization for Economic Co-operation and Development countries (OECD, 2020). Serving as a regional medical pole, Fortaleza receives patients from distant areas and faces a high demand on these equipments, since the entire Ceará state, with an area of nearly 149,000 km^2, has 55 magnetic resonance facilities, 0.3 equipment per 100,000 inhabitants.

Fortaleza discharges its wastewaters primarily by a submarine outfall located 3.2 km from the shoreline and secondly in two small rivers which cross the city which are under pressure of distinct human activities such as navigation, fishing and recreational activities. Here we investigated the concentrations of dissolved REE in Fortaleza estuaries and coastal waters in order to check whether Fortaleza medical activities lead to detectable anthropogenic Gd, to investigate potential wastewater-derived sources of contamination and to refine earlier mass balance calculations.

2. Materials and methods

2.1. Study area

Fortaleza climate is influenced by the Intertropical Convergence Zone (ITCZ) experiencing contrasted seasonal trade winds and rainfall regimes (Ferreira and da Silva Mello 2005). According to the national institute of meteorology (INMET 2019), 90% of the average total precipitation (1432 mm/year) occurs between January and June when the winds are relatively weak. Contrastingly, the period from July to December is dry and the winds are stronger. The prevailing winds are oriented WNW and generate average coastal currents parallel to the coast (Pereira et al., 2015). This circulation pattern has a relatively constant direction throughout the year as shown in Fig. 1a.

The city has approximately 2.7 million inhabitants (IBGE 2019) of which 61% have their wastewaters collected and treated (ANA 2017). Three water bodies cross the urban zone and receive treated and raw wastewaters discharges (Nilin et al., 2013): Cocó River, Ceará River and Maceió Stream (Fig. 1b). A high-capacity preliminary WWTP collects and treats 49% of the wastewaters produced by Fortaleza and discharges the effluents through a marine outfall built in the seventies. It is 3.2 km long, has a 1.5 m diameter and operates a 2.2 m^3 s^{-1} discharge at a 12m

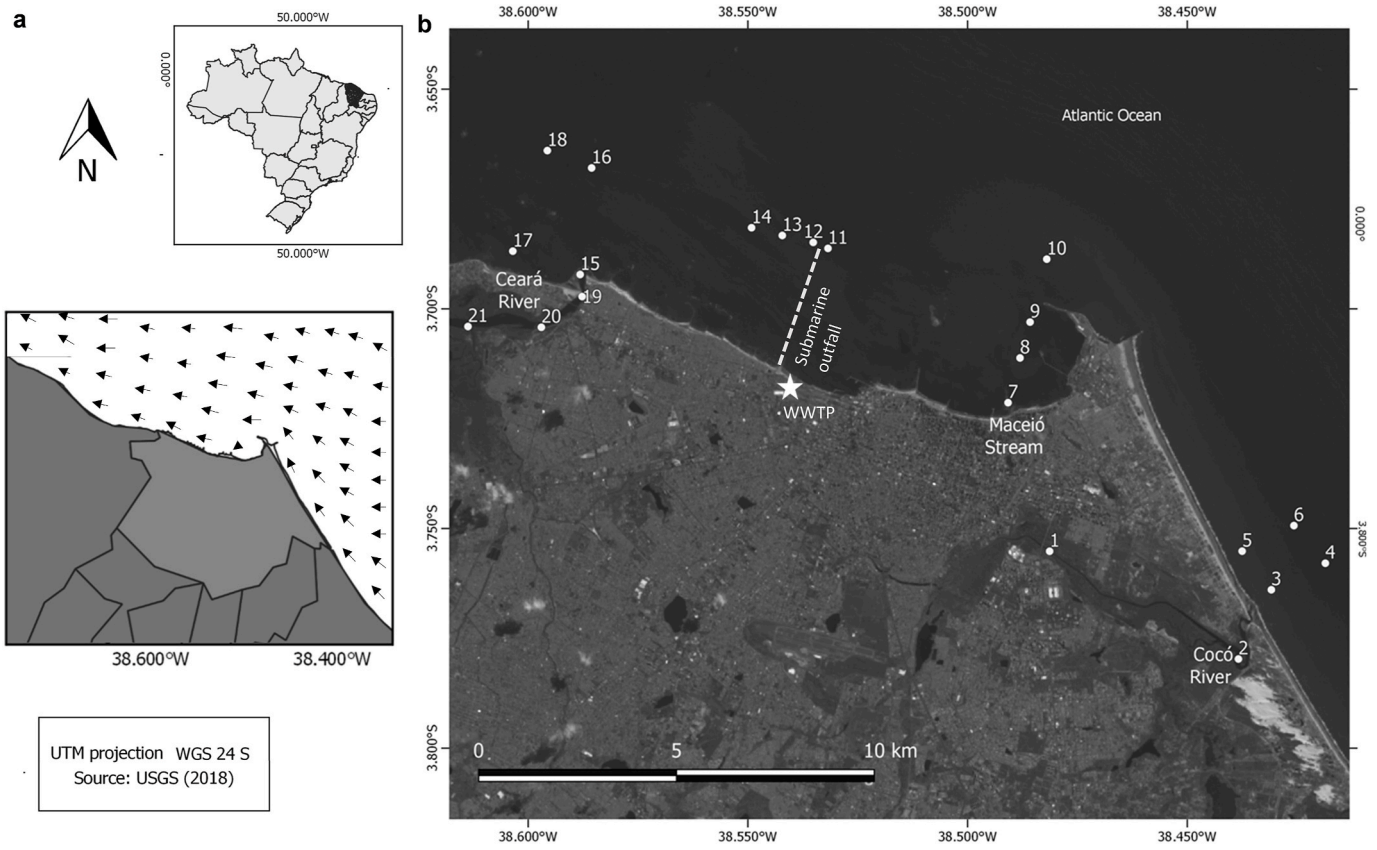

Fig. 1. Study area and sampling stations: a) Ceará state localization and Fortaleza coastal circulation scheme (current direction adapted from Pereira et al., 2015) b) Four areas were covered in this study: Cocó River (samples 1 to 6), Maceió Stream (samples 7 to 10), Fortaleza outfall (sample 11 to 14) and Ceará River (Sample 15 to 21). The dashed line represents the localization and extension of Fortaleza submarine outfall and the star the localization of the mmajor WWTP.

depth (CAGECE 2014). The coastal circulation maintains the wastewater plume distant from the shoreline and advects it parallel to the coast. In contrast, the waters from the Cocó and Ceará rivers, the Maceió Stream and the 32 storm sewers distributed alongside the city seafront are advected westwards but relatively close to the coast (Pereira et al., 2015).

2.2. Sampling

A total of 19 nearshore surface water samples were collected in April and May 2018 in areas under the influence of the Cocó and Ceará rivers, the Maceió Stream and the submarine outfall of Fortaleza (Fig. 1). Sampling points were chosen considering prevailing winds, water circulation and the subsequent urban water dispersion. Two bottom samples were also obtained at 12m in the outfall discharge area. Samples within the Cocó and Ceará rivers were also collected. Van Dorn bottles were used for sample collection and HCl cleaned 1L high-density polyethylene (HDPE) bottles were used for sample storage. Samples were filtered with pre-cleaned 0.45 μm cellulose ester mixed membranes (Millipore, Merck) and acidified with doubly distilled HCl (Quartz Subboiling distiller) to pH 2. Temperature and salinity data were acquired with an in situ multiparametric probe (EXO2, Ysi).

2.3. Analytical procedures

C18 solid-phase extraction cartridges (Sep-Pak, Waters), loaded with 2-ethylhexyl phosphate (HDMEP-H2DMEP), were used for REE preconcentration and salts removal (Shabani et al., 1992; Merschel et al., 2015; Amorim et al., 2019). Briefly samples were acidified, spiked and kept for a two months and a half period at ambient air conditioning lab temperature. Subsequently samples were loaded through the C18 cartridges with a peristaltic pump at a flow rate of 9 mL min^{-1}. Prior to the REE elution, the cartridges were washed with 10 mL of HCl 0.01 mol. L^{-1} at a flow rate of 3 mL min^{-1} to remove some major elements including the interfering Ba. Then, the analytes were eluted with 40 mL of HCl 5.6 mol.L^{-1}, at a flow rate of 3 mL min^{-1}. The eluate was evaporated in pre-cleaned 60-mL PFA vials on a heating plate until dryness and the remaining material was dissolved back in 5 mL of a 0.32 mol.L^{-1} HNO_3. All acids used in this extraction procedure were double-distilled.

Quantification of REE was carried out in an Agilent 7500ce inductively coupled plasma mass spectrometer (ICP-MS) according to analytical procedure for data treatment and interference monitoring/corrections proposed elsewhere (Rousseau et al., 2013; Amorim et al., 2019). REE concentrations were determined by isotopic dilution using a mix of ^{146}Nd, ^{151}Eu, and ^{172}Yb spikes added to the samples before the preconcentration step. In each individual sample the recoveries were monitored and corrected for Nd, Eu and Yb and interpolated for non-spiked REE. On average, Nd, Eu and Yb showed recoveries of 83%, 88%, and 86%, respectively. Blanks were inferior to 6% for heavy REE (HREE) and 3% for middle REE (MREE). For light REE (LREE) such as La, Ce, and Pr, blank correction reached about 10% of the signal in some samples. The methods for sample preparation and analyses used in this study were successfully applied the analyses of the SLRS-6 river water reference material (Amorim et al., 2019; Yeghicheyan et al., 2019). Considering the higher salinity of the samples investigated in the present study compared to SLRS-6, the matrix separation efficiency was checked by analyzing Na and Ca by Inductively Coupled Plasma Optical Emission Spectrometry (Thermo iCAP 6000 Series) and showed that preconcentrated samples had Na and Ca concentrations 10^6 and 2.10^2 times lower than seawater respectively. As discussed by de Campos and Enzweiler (2016) chelated Gd used as contrast agents can have low retention in C18 cartridges. Since our samples were kept acidified for a long period before preconcentration we assume good recoveries for this element. More analytical developments are however necessary in the field and specially to insure fully quantitative Gd recoveries for sea water. For example, a recent study on tap waters and soda samples by Schmidt et al. (2019) have shown good recoveries when adding a H_2O_2 digestion step prior to the acidification step.

3. Results

Table 1 shows the salinity, temperature and REE concentrations for the samples collected within the scope of this study. Temperature varied between 28.9 and 30.0 °C, salinity ranged from 0.3 for sample 1 (Cocó River estuary) to 36.0 for sample 15. Most of the coastal samples displayed salinities between 35.6 and 36 except for station 5 (32.8) which is influenced by the Cocó River plume. The saltiest samples presented values between 35.9 and 36.0 and can be considered as the marine endmember. Slightly fresher waters were observed for samples 11 and 12 (35.7 and 35.7, respectively) which are surface water samples located in the sewage outfall region characterized by a wastewater plume. Lower salinities were observed in Ceará River estuary (samples 19, 20 and 21; salinity 6.1, 7.8, and 19.2, respectively).

3.1. Rare earth elements

The sum of all REE concentration (∑REE) varied from 90.3 pmol kg^{-1} (coastal sample 6) to 1644 pmol kg^{-1} (sample 21). The highest ∑REE concentration were observed for Cocó and Ceará River estuaries which also presented low salinity (samples 1, 20 and 21). Post-Archean Australian Shale (PAAS) normalized REE diagrams (McLennan 1989) are reported in Fig. 2. Samples 1, 20 and 21, which presented the highest ∑REE levels, also showed REE distribution patterns with a substantial offset compared to the other samples (Fig. 2a and d). All REE distribution patterns displayed a gradual fractionation, from depleted LREE to enriched HREE. Atlantic Ocean waters usually display such typical fractionated behavior. Therefore, La_{sn}/Yb_{sn} ratios presented in Table 2 were systematically inferior to 1, varying from 0.09 for sample 1; with the lowest salinity sampled for Cocó River; to 0.59 for sample 11D located nearby the submarine outfall. Looking into detail, for most samples, however, REE patterns were rather flat from La to Nd and then increased from Nd to HREE. Sample 11D presented an enrichment in La (Fig. 2b) with a La_{sn}/Nd_{sn} ratio of 2 (Table 2). Cerium anomaly (Ce/Ce*) was calculated following equation (1):

$$\frac{Ce}{Ce^*} = \frac{Ce_{sn}}{(La_{sn} \times Pr_{sn})^{0.5}} \quad \text{Eq 1}$$

where Ce* is the estimated non anomalous cerium concentration, Ce_{sn}, La_{sn} and Pr_{sn} are the PAAS normalized REE concentrations. Ce/Ce* were on average 0.97 ± 0.16 and varied from 0.61 for Cocó River (sample 2) to 1.18 for sample 12S in the outfall area (Table 2). Samples 10 and 6 presented the lowest REE concentrations, with distribution patterns close to a sample collected by Rousseau et al. (2015) over the same continental margin further west at 90 m depth close to the Amazonian shelf break (Latitude: 2,26 °S e Longitude: −47,50 °W) (Figure S1). Despite this similarity in REE patterns, Ce displays a different behavior and while samples 6 and 10 indicate the absence of Ce anomaly (1.06 and 0.95, respectively) the sample reported for comparison displayed a large negative anomaly (0.5).

3.2. Gd anomaly

REE patterns presented an anomalous Gd behavior in many samples as it is offset from the smooth increasing trend in REE patterns (Fig. 2a–d). Several methods allow the numerical evaluation of the Gd anomaly by estimating the background shale normalized concentration (Gd_{sn}*) of this element (Hatje et al., 2016). Gd_{sn}* can be estimated by fitting, for each sample, a third-order polynomial of PAAS normalized REE values against their discrete ranking (from one to fifteen) and solving the equation for the Gd position (Figure S2). This multiple

Table 1
Sampling localization, hydrographic data and rare earth elements concentrations (pmol.kg^{-1}).

Area	Sample	Date	Latitude	Longitude	Temp.	Salinity	La	Ce	Pr	Nd	Sm	Eu	Gd	Tb	Dy	Ho	Er	Tm	Yb	Lu	∑REE
Cocó River	1	04/05/18	−3.75516	−38.48132	ND	0.3	118	177	35.5	172	42.2	10.9	154	5.9	37.8	11	46	8.9	76	16	910
	2	04/05/18	−3.77969	−38.43835	ND	35.3	25.9	31.2	5.43	23.0	4.70	1.29	7.79	1.1	8.1	2.0	6.8	1.1	7.2	1.3	127
	3	09/04/18	−3.75789	−38.41856	29.5	35.6	23.2	44.7	4.97	19.4	3.93	0.96	5.34	0.8	5.8	1.4	4.5	0.7	4.3	0.8	121
	4	09/04/18	−3.76393	−38.43086	29.4	35.7	21.7	42.1	4.41	17.6	3.66	1.00	5.10	0.8	5.4	1.2	4.3	0.6	4.0	0.6	112
	5	09/04/18	−3.75514	−38.43750	30.0	32.8	28.0	53.9	5.69	24.8	5.32	1.37	9.32	1.0	7.1	1.7	6.2	1.0	7.2	1.3	154
	6	09/04/18	−3.74932	−38.42572	29.3	35.8	18.1	36.2	3.46	12.7	2.86	0.75	3.61	0.6	4.0	0.9	3.1	0.5	3.0	0.5	90
Maceió Stream	7	13/04/18	−3.72134	−38.49077	29.4	35.9	26.0	41.1	4.83	19.5	3.91	1.05	6.12	0.9	6.3	1.5	5.2	0.8	5.4	0.9	124
	8	13/04/18	−3.71116	−38.48806	29.1	35.9	24.7	39.5	4.85	21.1	4.11	1.05	6.58	0.9	6.6	1.6	5.3	0.8	5.1	0.8	123
	9	13/04/18	−3.70299	−38.48577	28.9	36.0	25.0	40.2	4.82	19.5	4.02	1.06	6.14	0.9	6.5	1.5	5.2	0.8	5.3	0.8	122
	10	13/04/18	−3.68866	−38.48196	28.9	35.9	19.3	34.7	3.67	14.5	3.15	0.77	4.11	0.6	4.5	1.2	3.4	0.6	3.4	0.6	94
Fortaleza Outfall	11S	12/04/18	−3.68622	−38.53176	29.0	35.7	18.8	43.6	4.83	18.5	3.74	0.95	17.4	0.8	5.1	1.2	3.8	0.6	3.6	0.6	123
	11D	12/04/18	−3.68622	−38.53176	28.9	35.9	37.3	60.0	4.09	16.0	3.33	0.97	4.77	0.8	4.9	1.2	4.0	0.6	3.8	0.6	142
	12S	11/04/18	−3.68485	−38.53512	28.9	35.7	16.9	50.2	5.75	24.9	4.86	1.21	24.1	0.9	6.0	1.4	4.4	0.7	4.3	0.8	146
	12D	11/04/18	−3.68485	−38.53512	28.9	35.9	18.4	39.4	4.22	16.3	3.46	0.84	5.20	0.7	5.0	1.1	3.8	0.6	3.6	0.6	103
	13	11/04/18	−3.68327	−38.54216	29.1	35.7	16.1	42.3	4.82	20.9	4.18	1.10	16.9	0.8	5.4	1.3	4.2	0.6	4.1	0.7	123
	14	11/04/18	−3.68152	−38.54915	29.1	35.8	23.0	53.8	5.29	20.9	4.13	1.12	14.9	0.8	5.2	1.2	4.0	0.6	3.8	0.6	139
Ceará River	15	10/04/18	−3.69215	−38.58816	29.6	36.0	31.1	55.8	5.72	23.1	4.90	1.37	6.75	1.1	7.1	1.8	5.7	0.9	5.6	0.9	152
	16	10/04/18	−3.66790	−38.58555	29.3	36.0	22.0	42.4	3.83	14.4	3.06	0.81	4.04	0.6	4.1	1.0	3.2	0.5	3.0	0.5	103
	17	10/04/18	−3.68684	−38.60349	29.6	35.7	36.3	65.5	6.74	27.3	5.52	1.35	9.09	1.1	7.5	1.8	5.9	0.9	6.0	1.0	176
	18	10/04/18	−3.66395	−38.59563	29.34	35.6	26.5	49.4	5.76	23.3	4.73	1.30	8.61	1.0	6.1	1.5	4.7	0.8	4.6	0.9	139
	19	08/05/18	−3.69718	−38.58772	ND	19.2	39.6	58.9	8.44	35.9	7.30	1.93	11.0	1.4	9.3	2.2	8.0	1.3	9.1	1.7	196
	20	08/05/18	−3.70418	−38.59700	ND	7.8	272	664	67.1	283	53.4	13.0	62.1	7.3	41.8	9.2	31	5.1	38	7.5	1555
	21	08/05/18	−3.70399	−38.61369	ND	6.1	288	698	71.4	299	58.0	13.5	68.6	7.9	44.6	9.9	33	5.4	41	8.0	1645

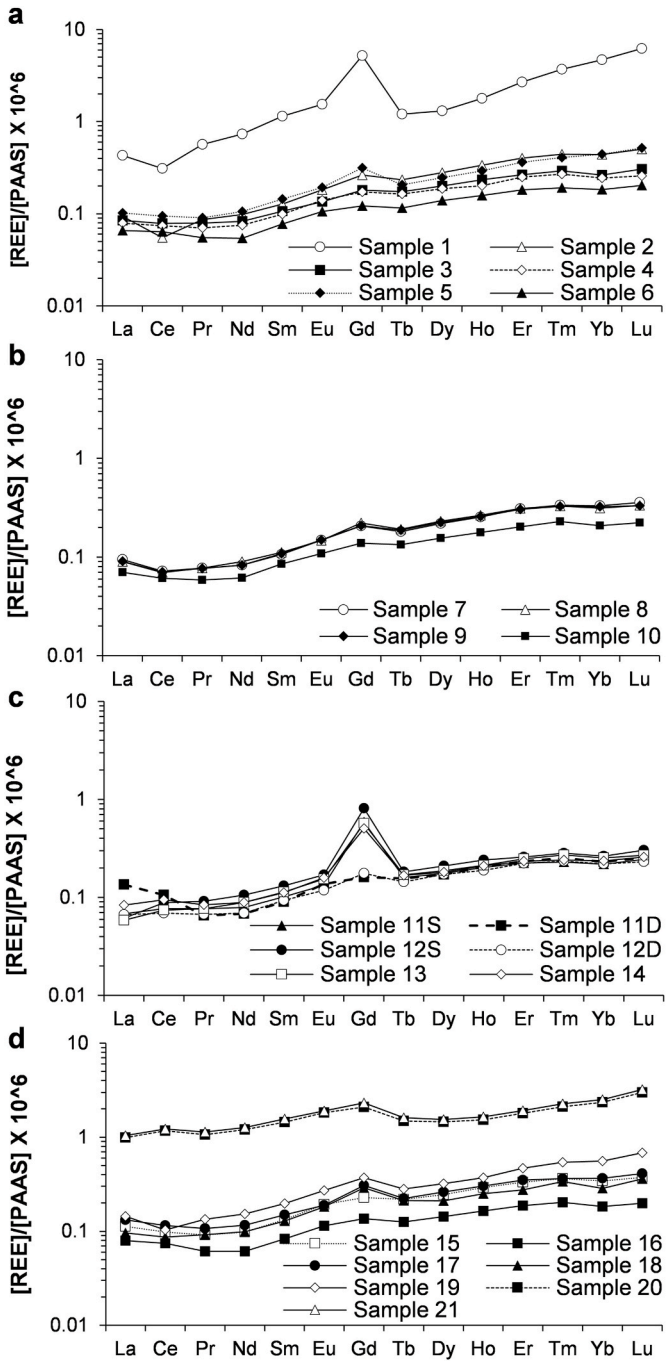

Fig. 2. PAAS normalized rare earth elements patterns in the areas investigated in this study: a) Cocó river, b) Maceió stream, c) Fortaleza submarine outfall, d) Ceará River.

regression method disregards potentially anomalous elements (Gd, Ce, and Eu). It is advantageous for not considering Gd as LREE nor HREE and thus more appropriated when comparing the range of REE patterns found between freshwater and seawater (Möller et al., 2002; Hatje et al., 2016). Gd anomaly (Gd_{sn}/Gd_{sn}^*) was calculated following equation (2):

$$\frac{Gd_{sn}}{Gd_{sn}^*} = \frac{Gd_{sn}}{(\beta_3 x^3 + \beta_2 x^2 + \beta_1 x + \beta_0)} \quad \text{Eq 2}$$

where Gd_{sn} is the PAAS normalized gadolinium concentration and Gd_{sn}^* is calculated by solving each fitted third-order polynomial of β_0, β_1, β_2 and β_3 parameters for x = 8 (gadolinium position). For low Gd_{sn}/Gd_{sn}^* values the anomaly can sometimes be hardly distinguishable from

Table 2
Post Archean Australian Shale (PAAS) normalized REE ratios, Ce and Gd anomalies, and anthropogenic Gd concentration (Gd_{anth}) expressed in pmol. kg^{-1}.

Area	Sample	$\frac{La_{sn}}{Yb_{sn}}$	$\frac{La_{sn}}{Nd_{sn}}$	$\frac{Ce_{sn}}{Ce^{*}_{sn}}$	$\frac{Gd_{sn}}{Gd^{*}_{sn}}$	Gd_{anth}
Cocó River	1	0.09	0.59	0.63	5.4	125.37
	2	0.21	0.96	0.61	1.3	1.77
	3	0.32	1.02	0.96	1.2	0.76
	4	0.32	1.05	0.99	1.2	0.84
	5	0.23	0.96	0.99	1.7	3.88
	6	0.36	1.22	1.06	1.2	0.50
Maceió Stream	7	0.29	1.14	0.85	1.3	1.36
	8	0.29	1.00	0.83	1.3	1.46
	9	0.28	1.09	0.85	1.2	1.20
	10	0.34	1.14	0.95	1.2	0.57
Fortaleza Outfall	11S	0.31	0.87	1.06	4.1	13.18
	11D	0.59	1.99	1.12	1.3	1.01
	12S	0.23	0.58	1.18	4.7	18.94
	12D	0.30	0.97	1.03	1.3	1.27
	13	0.23	0.66	1.11	3.7	12.28
	14	0.35	0.94	1.13	3.4	10.53
Ceará River	15	0.33	1.15	0.97	1.2	1.11
	16	0.43	1.3	1.07	1.2	0.72
	17	0.36	1.14	0.97	1.5	3.14
	18	0.34	0.97	0.93	1.7	3.47
	19	0.26	0.94	0.74	1.5	3.73
	20	0.42	0.82	1.14	1.6	22.04
	21	0.42	0.82	1.13	1.6	25.58

natural Gd levels as this REE is located between LREE and HREE which may have contrasted reactivity and fractionation patterns and because of possible analytical uncertainties in REE determination. As a result, it is important to consider low positive Gd anomalies with caution and a threshold for Gd_{sn}/Gd_{sn}^{*} between 1.3 and 1.5 is usually chosen arbitrarily to attribute the anomaly to anthropogenic activities (Pedreira et al., 2018; Andrade et al., 2020). In our study considering $Gd_{sn}/Gd_{sn}^{*} \geq 1.3$, 16 samples presented a Gd anomaly and considering $Gd_{sn}/Gd_{sn}^{*} \geq 1.4$, 11 samples presented this anomaly (Table 2). The sample from the Cocó River presenting the lowest salinity (sample 1) also displayed the highest Gd/Gd* anomaly. In the coastal area influenced by the Cocó River estuary, only sample 5 displayed an anomalous behavior. In the Ceará River, estuarine samples 19, 20 and 21 and coastal samples 17 and 18 displayed a positive anomaly. In the Maceió Stream coastal area, samples 7 and 8 showed a slight positive anomaly. All the surface samples in the outfall area presented a significant positive anomaly ranging from 3.4 to 4.1, it is comparable with the value of 3.4 found by Pedreira et al. (2018) for the outfall plume of Salvador city.

3.3. Robustness of the polynomial method for Gd* estimates

Since La can eventually present an anomalous behavior compared to other LREE (Kulaksız and Bau 2011; Garcia-Solsona et al., 2014; Klaver et al., 2014; Amorim et al., 2019) we made a sensitivity test in order to evaluate any possible influence of La variations on Gd* estimations (Figure S3a). For sample 3, a −50% and +50% variation of La value leads to a 3.5% variation of Gd* in the opposite direction (Figure S3b). Consequently, this third order polynomial method can be applied thoroughly for Gd* estimations except in the presence of very high La anomalies (i. e., more than 10-fold the non anomalous concentration). In our study, La behavior was quite constant for most of the samples with narrow variations of La_{sn}/Pr_{sn} (1.10 ± 0.27). The only sample showing a contrasted La behavior was sample 11D (Fig. 2c), which presented a La_{sn}/Pr_{sn} ratio of 2 and a slightly anomalous Gd/Gd* ratio of 1.3. If we fit a polynomial for this sample using a hypothetical La_{sn} value using the average La_{sn}/Pr_{sn} value of 1.05 we find a different Gd/Gd* of 1.6. Beside this exception where the Gd anomaly could be slightly underestimated, the polynomial method is suitable and allows us to compare our data with other studies (Hatje et al., 2016; Pedreira et al., 2018; Andrade et al., 2020).

4. Discussion

4.1. Fortaleza as a traceable source of anthropogenic Gd

The Gd/Gd* values we observe ranged from 1.2 to 5.4 and are comparable with previously reported values in coastal waters near Salvador (Gd/Gd* ranging from 1 to 3.4; Pedreira et al., 2018) but substantially lower than values observed in continental waters near other Brazilian metrocities like Campinas city in fluvial environment (Gd/Gd* ranging from 0.8 to 86.7; De Campos and Enzweiler et al., 2016) and Brasilia's lake (Gd/Gd* ranging from 1.1 to 68.4; Merschell et al., 2015; Amorim et al., 2019). Considering that the highest ratios were observed in Cocó and Ceará rivers and in the WWTP outfall region, Fortaleza unequivocally provides a traceable source of anthropogenic Gd to the ocean. Several magnetic resonance equipments are implanted in Fortaleza and this medical care activity has been the most suitable candidate to explain Gd anomalies in the waterbodies draining densely populated areas. Thus, it is likely that Gd anomalies are linked to the use of Gd-CAs.

We also observe significant Gd anomalies in samples collected westwards of the Cocó River (sample 5), the Ceará River (sample 17) and the outfall region (samples 12, 13 and 14), suggesting a Gd mobility and dispersion patterns in agreement with the ones modelled by Pereira et al. (2015). It is important to point out that as Gd/Gd* ratios relate to the background Gd concentrations they are not fully adequate for comparisons between continental waters and seawaters which display large variations in REE levels. Additionally, these elements are reactive and can be removed from the dissolved phase by scavenging and colloids flocculation or added to the system through release from sediments and suspended particles (Sholkovitz 1993; Rousseau et al., 2015; Johannesson et al., 2017).

4.2. Anthropogenic gadolinium quantification

To overcome the effect of potentially high natural REE variation on Gd/Gd*ratios, for example between riverwater and seawater, we estimate the absolute anthropogenic gadolinium concentration (Gd_{anth}) using equation (3):

$$Gd_{anth} = Gd - \left(Gd_{PAAS} \times Gd^{*}_{sn}\right) \quad \text{Eq. 3}$$

where Gd is the measured concentration, Gd_{PAAS} is the PAAS normalized Gd concentration, as proposed by McLennan (1989), and Gd_{sn}^{*} stands for the PAAS normalized natural Gd estimated by the polynomial fit. As

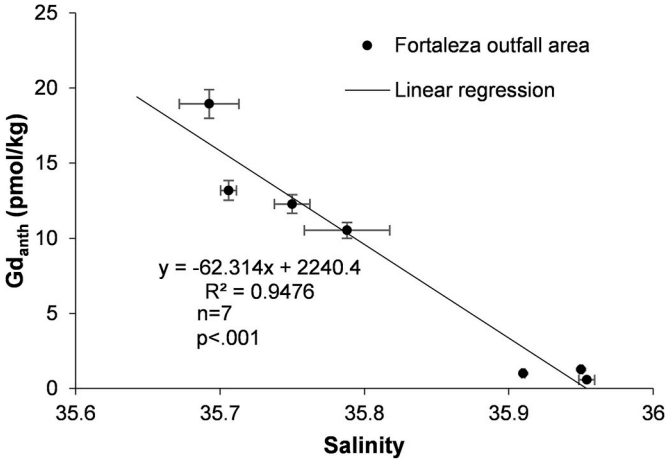

Fig. 3. Anthropogenic gadolinium (Gd_{anth}) as function of salinity in Fortaleza submarine outfall area.

shown in Fig. 3 Gd_{anth} decreases as salinity increases in the outfall region (samples 10, 11S, 11D, 12S, 12D, 13, and 14) reflecting the dilution of a concentrated freshwater endmember by seawater. In the Cocó River area (samples 1, 2, and 5) and in the Ceará River area (samples 19, 20, and 21) the same dilution pattern is observed (figure S4). A remarkably linear and conservative estuarine Gd_{anth} behavior was previously reported for the entire salinity gradient in the Weser estuary (Kulaksız and Bau 2007). This is in agreement with our results in the outfall region where there was a significant negative correlation between salinity and Gd_{anth} ($r^2(7) = 0.95$, $p < .001$). Assuming a conservative Gd_{anth} behavior over the entire salinity gradient, one can infer that the wastewater endmember concentration ($Gd_{anth,\ wwtp}$) is the interception of the linear regression with the Y axis at 0 salinity (i. e., the $\widehat{b}$ parameter). The standard deviation (s_b) of the intercept $\widehat{b}$ is the square root of its variance (Equation (4)):

$$s_b^2 = \frac{SS_E}{n-2}\left(\frac{1}{n} + \frac{\bar{x}^2}{SS_{xx}}\right) \quad \text{Eq 4}$$

where SS_E is sum of squared estimate of errors, SS_{xx} is sum of squares of x observations. According to Eq. (4), s_b allows us to give a 95% confidence interval for $\widehat{b}$ following the t-distribution with n-2 degrees of freedom. As a result, we calculate a source concentration for the Gd_{anth} signal measured in the outfall area of 2240 ± 470 pmol kg^{-1}. This result is in agreement with the value obtained by Pedreira et al. (2018) in Salvador city, where the authors reported Gd_{anth} values measured directly in the WWTPs and varying between 900 and 2605 pmol kg^{-1}. These values were used as reference to estimate Gd_{anth} exported from the Brazilian coastal cities. Considering the average discharge of the submarine outfall of Fortaleza, approximately 24.6 ± 5.2 kg of anthropogenic Gd are launched to the ocean every year. It corresponds to nearly 22,400 MRI exams if an average of 1.1 g of Gd is administered during each analysis in Brazil (Telgmann et al., 2013; Merschel et al., 2015; Pedreira et al., 2018). Our estimate is based on a synoptic observation and shall be considered more as an order of magnitude, indeed substantial variations in Gd concentrations can occur in WWTP within a few days according to the daily number of MRI exams (Pedreira et al., 2018).

For the estuaries of Cocó and Ceará rivers, the Gd_{anth} values extrapolated to the freshwater endmember ($Gd_{anth,S=0}$) were of 126 ± 5 pmol kg^{-1} and 35.2 ± 1.2 pmol kg^{-1}, respectively. Despite higher Gd/Gd* ratios and Gd_{anth} values within the estuary, these $Gd_{anth}(0)$ levels are inferior to the one calculated for the submarine outfall and support the hypothesis that wastewater discharges are firstly diluted by the river waters prior to seawater/river mixing. According to the Brazilian National Water Agency (ANA 2017) Cocó and Ceará rivers receive, respectively, a total of 352 L s^{-1} and 104 L s^{-1} of treated and non-treated wastewaters. These effluents are distributed in several punctual canalizations along the watercourses. To our knowledge, yearly hydrological data are not available for both rivers and the only data accessible from the water agency is their minimum reference discharge (76.5 L s^{-1} for Cocó River and 116.6 L s^{-1} for Ceará River). As a result, during the dry season, it is estimated that wastewaters shall account for 75% and 40% of Cocó and Ceará rivers discharge. As sampling was carried out during the rainy season (April and May) both rivers shall display a substantially higher discharge than during the dry season. In this case, a simple mass balance can be applied here to estimate the river water and wastewater (%WW) proportions during the sampling period using equation (5):

$$\%WW = \frac{Gd_{anth\ ,S=0}}{Gd_{anth,WWTP}} \quad \text{Eq. 5}$$

where $Gd_{anth\ ,S=0}$ is the anthropogenic Gd estimated for the freshwater endmember and $Gd_{anth,WWTP}$ is the anthropogenic Gd concentration within the wastewater treatment plant.

Based on equation (5) and considering the minimum and maximum values for $Gd_{anth,WWTP}$ as observed by Pedreira et al. (2018), i. e., 900–2600 pmol kg^{-1}, we suggest that wastewaters accounts for 4.8%–14% of the discharge of Cocó River and for 1.4%–3.9% of the Ceará River during the study period. Therefore, Gd_{anth} is a suitable tracer to monitor the dilution of wastewaters within rivers as it is minimally influenced by wastewater treatment processes compared to other usual parameters such as biologic oxygen demand and nutrients. In addition, Gd_{anth} might closely follow the fate of other conservative emerging contaminants. The marine outfall delivers high Gdanth concentrations rapidly diluted by seawater. Contrastingly, for river systems, even-though conservative contaminants are previously diluted within freshwater prior mixing with seawater, they might be more harmful to the biota in estuaries given their longer residence time and higher absolute concentrations.

4.3. Potential applications using Gd_{anth} as a conservative tracer

In this section we develop a simple conceptual vision of Gd_{anth} in salinity gradients and revisit earlier studies based on this approach. Considering the conservative behavior of Gd_{anth} during freshwater/seawater mixing, three scenarios can possibly occur. In the first scenario (Fig. 4a), a concentrated $Gd_{anth,\ S=0}$ source is diluted by seawater. This high Gd_{anth} content is characteristic of wastewater outfalls and can be applied to evaluate endmember concentrations and fluxes or to attribute confidently eventual slight salinity fluctuations due to the presence of diluted sewage plumes. Samples collected in the present study in the Fortaleza outfall area and in Salvador city outfall area by Pedreira et al. (2018) can be associated with this scenario.

In scenario two (Fig. 4b), a freshwater source with lower and homogeneous Gd_{anth} levels mixes with seawater. In this scenario, any concentrated source is mixed and diluted by freshwaters (i.e. 0 salinity) prior to mixing with seawater. This scenario is observable for river samples collected in Cocó and Ceará rivers in the present study and allows to calculate water balances. This type of estuarine mixing was also observed for the Weser estuary where seasonal variations of wastewater dilution in the freshwater endmember are observable between March 2005 (Gd_{anth} = 86 ± 4 pmol kg^{-1}) and November 2005 (Gd_{anth} = 137 ± 1 pmol kg^{-1}) as shown in Fig. 5a (Kulaksız and Bau 2007).

In a third scenario (Fig. 4c), two distinct freshwater sources with different Gd_{anth} concentrations are mixed with seawater, this can lead in two distinct Gd_{anth} vs Salinity behavior within the same area. It is the case for the San Francisco Bay study by Hatje et al. (2016). Indeed, by representing the concentrations of Gd_{anth} using their dataset (Fig. 5b), it is possible to observe two distinct freshwater/seawater conservative mixing patterns. In the northern part of the Bay, by extrapolating Gd_{anth} to part the 0 salinity we obtain 35.1 ± 2.5 pmol kg^{-1}, which is likely to represent Sacramento River Gd_{anth} concentration at the time of sampling. On the other hand, in the southern part of the Bay, we estimate a substantially higher freshwater source of Gd_{anth} (853 ± 83 pmol kg^{-1}). This higher level shall correspond to the contribution of WWTP, as four cities located around the southern part of the Bay contributes with WWTP discharges (Palo Alto, San José, Redwood and San Leandro).

Finally, the conservative behavior of Gd_{anth} during estuarine freshwater/seawater mixing can help us identify sources and fate of wastewater and its compounds. The recent study by Andrade et al. (2020) in the Todos os Santos Bay of Salvador showed minor to negligible Gd_{anth} values within the bay except in its eastern portion where a 12h time station was made (Fig. 5c). Two relations between Gd_{anth} and salinity appear: from the high to the low tide, the white diamonds indicate a freshwater endmember with highly concentrated Gd_{anth} values of 350 ± 46 pmol kg^{-1}. In contrast, during the rising tide, a mixing with salty and Gd_{anth} rich waters occurs (black triangles). It is likely that these salty Gd_{anth}-rich waters were originated outside the bay by mixing of waste water from the outfalls of Salvador (located outside the bay, near its entrance) with Atlantic waters. If we perform a mass balance using Pedreira et al. (2018) data for the marine endmember (S = 36.8) and WWTP Gd_{anth} concentrations (900–2600 pmol kg^{-1}), waters having

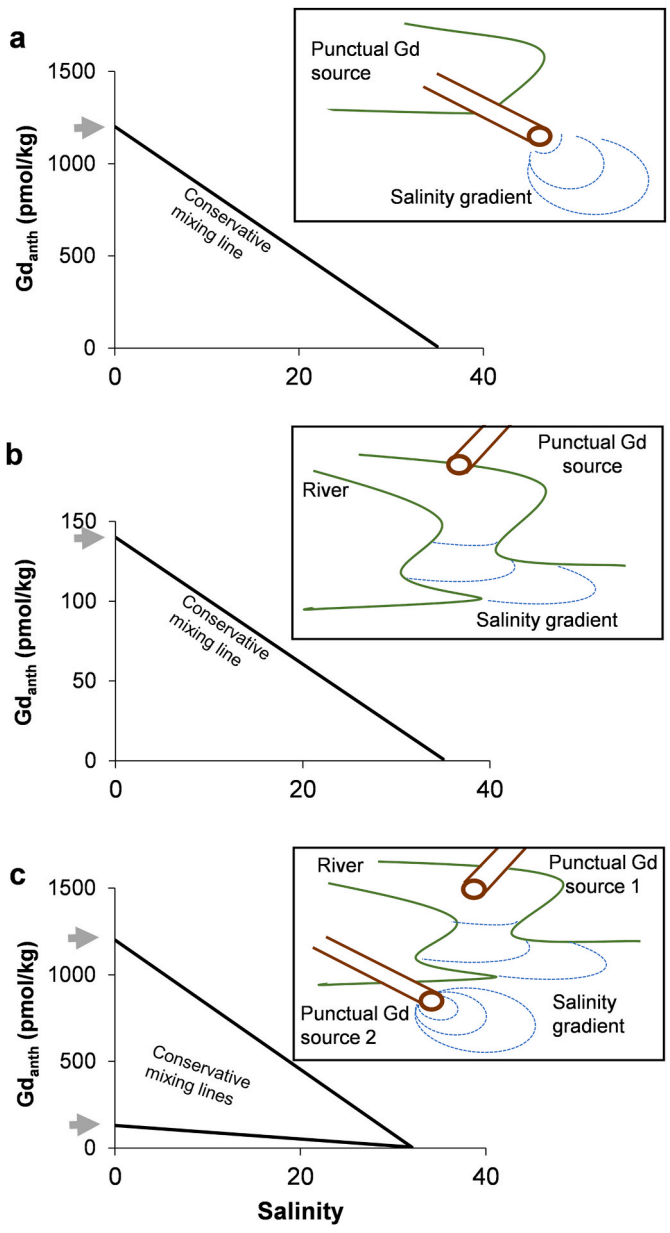

Fig. 4. Conceptual cases illustrating the conservative behavior of anthropogenic Gd during freshwater/seawater mixing: a) highly concentrated Gd_{anth} source scenario; b) diluted Gd_{anth} source scenario and; c) two distinct sources scenarios.

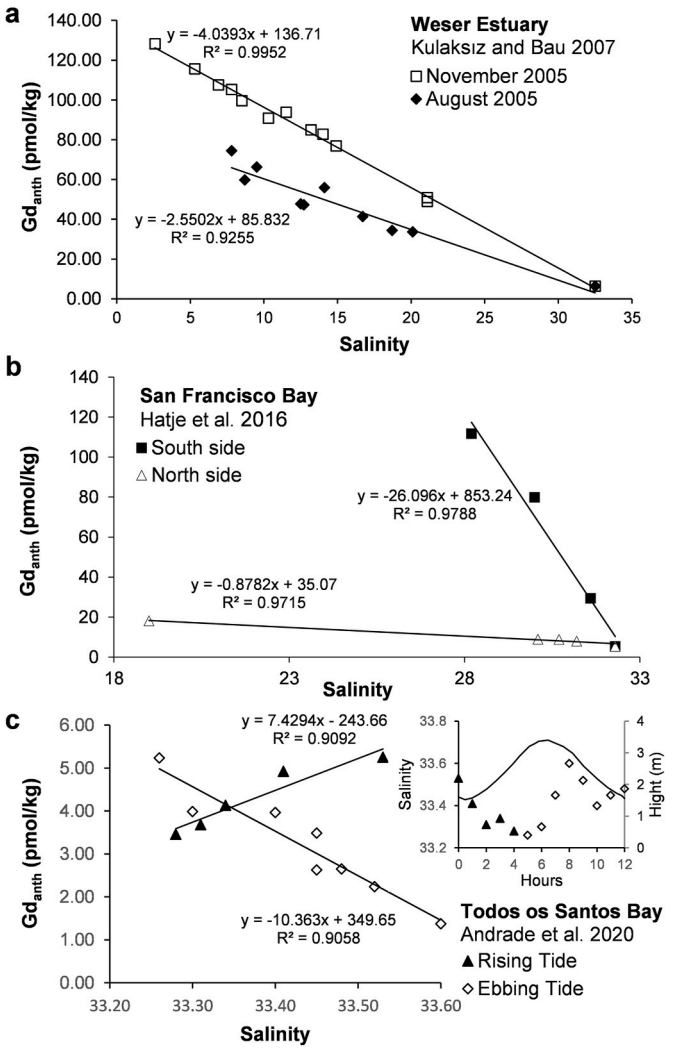

Fig. 5. Anthropogenic gadolinium (Gd_{anth}) in: a) the Weser estuary (Kulaksız and Bau 2007); b) the San Francisco Bay (Hatje et al., 2016) and c) the Todos os Santos Bay (Andrade et al., 2020).

36.15 ± 0.3 salinity and 25 ± 6 pmol kg^{-1} of Gd_{anth} (i.e. waters containing 1–2% waste waters) entered the bay to mix with fresher inner bay waters.

5. Conclusions

We observed positive Gd anomalies at the WWTP submarine outfall of the city of Fortaleza. This excess of Gd has an anthropogenic origin and is mostly associated with renal excretion of chelated Gd used as a contrasting agent in magnetic resonance imaging. We calculated the absolute concentration of Gd_{anth} and, considering its conservative behavior, we estimated that wastewaters from the WWTP have a Gd_{anth} concentration of 2.2 ± 0.5 nmol kg^{-1} and delivers annually approximately 25 kg of Gd to the Atlantic Ocean. This load represents roughly half of city's total Gd disposal since the submarine outfall transports 49.1% of Fortaleza wastewaters. A large part of the other half of the Gd disposal reaches two rivers which receive wastewater discharges from the city of Fortaleza and diluting Gd prior to the freshwater/seawater mixing. Using a simple mass balance, we observed that Gd_{anth} is a suitable tool to trace and monitor wastewaters dynamics and dilution in Fortaleza, being potentially helpful for decision and policies making in water management. Further studies are however necessary for such purpose in order to refine the quantitative estimates of source concentration and hydrological variability and thoroughly calibrate this tracer. Moreover, one can infer that the number of MRI analyses have been drastically reduced worldwide during the COVID-19 Pandemic. Regarding conservative contaminants, sewage shall present substantially higher threats to biota if launched in river and estuaries than by marine outfalls as even if diluted, they show higher spatial confinement, longer residence time and higher absolute levels in estuaries. The conservative behavior of both salinity and Gdanth allowed us to classify the mixing of urban water/seawater in three distinct scenarios, this systematic shall be useful for applications in several other coastal cities and estuaries with upstream anthropic impact. Increasing the monitoring of this contaminant of emerging concern is important as MRI analyses are facing a constant grow, and little is known regarding its toxicity and the processes that may act as a sink for Gdanth. Finally, this tracer could also be applied as a forensic tool to monitor anthropogenic contamination of source and groundwater polluted by leaking of raw sewage pipes or to

detect clandestine wastewater connections to storm sewers in Brazilian cities.

Declaration of competing interest

The authors declare that they have no known competing financial interests or personal relationships that could have appeared to influence the work reported in this paper.

Acknowledgments

FUNCAP [Grant PRONEM PNE 0112-00007.01.00/16] and CNPq [Grant number 454494/2014-9] Brazilian agencies are thanked for funding, the National Institute of Criminalistic of Brazilian Federal Police for providing access to the ICP-MS, Crisiana Andrade and Cleidiane Gomes from the Nutec laboratory are thanked for lab facilities and ICP-OES access. Finaly we thank Bárbara Pereira Paiva, Erika Roanna da Silva and Rozane Marins.

Appendix A. Supplementary data

Supplementary data to this article can be found online at https://doi.org/10.1016/j.apgeochem.2021.104908.

References

Amorim, A.M., Sodré, F.F., Rousseau, T.C.C., Maia, P.D., 2019. Assessing rare-earth elements and anthropogenic gadolinium in water samples from an urban artificial lake and its tributaries in the Brazilian Federal District. Microchem. J. 148 https://doi.org/10.1016/j.microc.2019.04.055.

Ana, 2017. Atlas esgotos: despoluição de bacias hidrográficas/Agência Nacional de Águas. Secretaria Nacional de Saneamento Ambiental. - Brasília: ANA.

Andrade, R.L.B., Hatje, V., Pedreira, R.M.A., et al., 2020. REE fractionation and human Gd footprint along the continuum between Paraguaçu River to coastal South Atlantic Waters. Chem. Geol., 119303

Bau, M., Dulski, P., 1996. Anthropogenic origin of positive gadolinium anomalies in river waters. Earth Planet Sci. Lett. 143, 245–255.

Bau, M., Knappe, A., Dulski, P., 2006. Anthropogenic gadolinium as a micropollutant in river waters in Pennsylvania and in Lake Erie, northeastern United States. Chemie der erde-Geochemistry 66, 143–152.

CAGECE, 2014. Diagnóstico do Sistema de Esgotamento Sanitário.

Coppin, F., Berger, G., Bauer, A., et al., 2002. Sorption of lanthanides on smectite and kaolinite. Chem. Geol. 182, 57–68.

Datasus, 2019. Cadastramento Nacional de Estabelecimentos de Saúde – CNES. Relatórios-Equipamentos - Ministerio da saúde. http://cnes2.datasus.gov.br. (Accessed 23 November 2019).

de Campos, F.F., Enzweiler, J., 2016. Anthropogenic gadolinium anomalies and rare earth elements in the water of Atibaia River and Anhumas Creek, Southeast Brazil. Environ. Monit. Assess. 188, 281.

Elderfield, H., 1988. The oceanic chemistry of the rare-earth elements. Philos Trans R Soc London Ser A, Math Phys Sci 325, 105–126.

Feng, X., Xia, Q., Yuan, L., et al., 2010. Impaired mitochondrial function and oxidative stress in rat cortical neurons: implications for gadolinium-induced neurotoxicity. Neurotoxicology 31, 391–398.

Ferreira, A.G., da Silva Mello, N.G., 2005. Principais sistemas atmosféricos atuantes sobre a região Nordeste do Brasil e a influência dos oceanos Pacífico e Atlântico no clima da região. Rev Bras Climatol 1.

Fujita, Y., Walton, M., Das, G., et al., 2020. Impacts of anthropogenic gadolinium on the activity of the ammonia oxidizing bacterium Nitrosomonas europaea. Chemosphere 127250.

Garcia-Solsona, E., Jeandel, C., Labatut, M., et al., 2014. Rare earth elements and Nd isotopes tracing water mass mixing and particle-seawater interactions in the SE Atlantic. Geochem. Cosmochim. Acta 125, 351–372.

Hatje, V., Bruland, K.W., Flegal, A.R., 2016. Increases in anthropogenic gadolinium anomalies and rare earth element concentrations in San Francisco Bay over a 20 year record. Environ. Sci. Technol. 50, 4159–4168.

Henderson, P., 1984. General geochemical properties and abundances of the rare earth elements. Developments in Geochemistry. Elsevier, pp. 1–32.

Henriques, B., Coppola, F., Monteiro, R., et al., 2019. Toxicological assessment of anthropogenic Gadolinium in seawater: biochemical effects in mussels Mytilus galloprovincialis. Sci. Total Environ. 664, 626–634.

IBGE, 2019. Informações gerais sobre Fortaleza. https://www.ibge.gov.br/cidades-e-estados/ce/fortaleza.html. (Accessed 15 December 2019).

INMET, 2019. Normais Climatológicas Do Brasil. http://www.inmet.gov.br/. (Accessed 15 December 2019).

Johannesson, K.H., Palmore, C.D., Fackrell, J., et al., 2017. Rare earth element behavior during groundwater–seawater mixing along the Kona Coast of Hawaii. Geochem. Cosmochim. Acta 198, 229–258.

Klaver, G., Verheul, M., Bakker, I., et al., 2014. Anthropogenic rare earth element in rivers: gadolinium and lanthanum. Partitioning between the dissolved and particulate phases in the Rhine River and spatial propagation through the rhine-meuse delta (The Netherlands). Appl. Geochem. 47, 186–197.

Köhler, S.J., Harouiya, N., Chaïrat, C., Oelkers, E.H., 2005. Experimental studies of REE fractionation during water–mineral interactions: REE release rates during apatite dissolution from pH 2.8 to 9.2. Chem. Geol. 222, 168–182.

Kulaksız, S., Bau, M., 2007. Contrasting behaviour of anthropogenic gadolinium and natural rare earth elements in estuaries and the gadolinium input into the North Sea. Earth Planet Sci. Lett. 260, 361–371. https://doi.org/10.1016/j.epsl.2007.06.016.

Kulaksız, S., Bau, M., 2011. Rare earth elements in the Rhine River, Germany: first case of anthropogenic lanthanum as a dissolved microcontaminant in the hydrosphere. Environ. Int. 37, 973–979.

Kümmerer, K., Helmers, E., 2000. Hospital effluents as a source of gadolinium in the aquatic environment. Environ. Sci. Technol. 34, 573–577.

Lawrence, M.G., 2010. Detection of anthropogenic gadolinium in the brisbane river plume in moreton bay, queensland, Australia. Mar. Pollut. Bull. 60, 1113–1116.

Lerat-Hardy, A., Coynel, A., Dutruch, L., et al., 2019. Rare Earth Element fluxes over 15 years into a major European Estuary (Garonne-Gironde, SW France): hospital effluents as a source of increasing gadolinium anomalies. Sci. Total Environ. 656, 409–420.

Luo, Y.-R., Byrne, R.H., 2004. Carbonate complexation of yttrium and the rare earth elements in natural waters. Geochem. Cosmochim. Acta 68, 691–699.

McLennan, S.M.S.M., 1989. Rare earth elements in sedimentary rocks: influence of provenance and sedimentary processes. Geochemistry Mineral Rare Earth Elem Rev Mineral 21 (21), 169–200.

Merschel, G., Bau, M., Baldewein, L., et al., 2015. Tracing and tracking wastewater-derived substances in freshwater lakes and reservoirs: anthropogenic gadolinium and geogenic REEs in Lake Paranoá, Brasilia. Compt. Rendus Geosci. 347, 284–293. https://doi.org/10.1016/j.crte.2015.01.004.

Möller, P., Dulski, P., Bau, M., et al., 2000. Anthropogenic gadolinium as a conservative tracer in hydrology. J. Geochem. Explor. 69, 409–414.

Möller, P., Paces, T., Dulski, P., Morteani, G., 2002. Anthropogenic Gd in surface water, drainage system, and the water supply of the city of Prague, Czech Republic. Environ. Sci. Technol. 36, 2387–2394.

Mortatti, B.C., Enzweiler, J., 2019. Major ions and rare earth elements hydrogeochemistry of the Atibaia and Jaguari rivers subbasins (Southeast Brazil). Appl. Geochem. 111, 104461.

Nilin, J., Moreira, L.B., Aguiar, J.E., et al., 2013. Sediment quality assessment in a tropical estuary: the case of Ceará River, Northeastern Brazil. Mar. Environ. Res. 91, 89–96.

Nozaki, Y., Lerche, D., Alibo, D.S., Tsutsumi, M., 2000. Dissolved indium and rare earth elements in three Japanese rivers and Tokyo Bay: evidence for anthropogenic Gd and in. Geochem. Cosmochim. Acta 64, 3975–3982.

OECD, 2020. Magnetic Resonance Imaging (MRI) Units. https://data.oecd.org/healtheqt/magnetic-resonance-imaging-mri-units.htm. (Accessed 29 April 2020).

Oksendal, A.N., Hals, P., 1993. Biodistribution and toxicity of MR imaging contrast media. J. Magn. Reson. Imag. 3, 157–165.

Pałasz, A., Czekaj, P., 2000. Toxicological and cytophysiological aspects of lanthanides action. Acta Biochim. Pol. 47, 1107–1114.

Pedreira, R.M.A., Pahnke, K., Böning, P., Hatje, V., 2018. Tracking hospital effluent-derived gadolinium in Atlantic coastal waters off Brazil. Water Res. 145, 62–72.

Pereira, S.P., Rosman, P.C.C., Alvarez, C., et al., 2015. Modeling of coastal water contamination in Fortaleza (Northeastern Brazil). Water Sci. Technol. 72, 928–936.

Rabiet, M., Letouzet, M., Hassanzadeh, S., Simon, S., 2014. Transmetallation of Gd-DTPA by Fe3+, Cu2+ and Zn2+ in water: batch experiments and coagulation–flocculation simulations. Chemosphere 95, 639–642.

Rousseau, T.C.C., Sonke, J.E., Chmeleff, J., et al., 2015. Rapid neodymium release to marine waters from lithogenic sediments in the Amazon estuary. Nat. Commun. 6 https://doi.org/10.1038/ncomms8592.

Rousseau, T.C.C., Sonke, J.E., Chmeleff, J., et al., 2013. Rare earth element analysis in natural waters by multiple isotope dilution-sector field ICP-MS. J Anal At Spectrom 28. https://doi.org/10.1039/c3ja30332b.

Schijf, J., Christy, I.J., 2018. Effect of Mg and Ca on the stability of the MRI contrast agent Gd–DTPA in seawater. Front Mar Sci 5, 111.

Schmidt, K., Bau, M., Merschel, G., Tepe, N., 2019. Anthropogenic gadolinium in tap water and in tap water-based beverages from fast-food franchises in six major cities in Germany. Sci. Total Environ. 687, 1401–1408.

Shabani, M.B., Akagi, T., Masuda, A., 1992. Preconcentration of trace rare-earth elements in seawater by complexation with bis (2-ethylhexyl) hydrogen phosphate and 2-ethylhexyl dihydrogen phosphate adsorbed on a C18 cartridge and determination by inductively coupled plasma mass spectrometry. Anal. Chem. 64, 737–743.

Shellock, F.G., 2000. Magnetic Resonance Procedures: Health Effects and Safety. Crc Press.

Sholkovitz, E.R., 1993. The geochemistry of rare earth elements in the Amazon River estuary. Geochem. Cosmochim. Acta 57, 2181–2190.

Sholkovitz, E.R., Landing, W.M., Lewis, B.L., 1994. Ocean particle chemistry: the fractionation of rare earth elements between suspended particles and seawater. Geochem. Cosmochim. Acta 58, 1567–1579.

Telgmann, L., Sperling, M., Karst, U., 2013. Determination of gadolinium-based MRI contrast agents in biological and environmental samples: a review. Anal. Chim. Acta 764, 1–16.

Tepe, N., Romero, M., Bau, M., 2014. High-technology metals as emerging contaminants: strong increase of anthropogenic gadolinium levels in tap water of Berlin, Germany, from 2009 to 2012. Appl. Geochem. 45, 191–197.

Xia, Q., Feng, X., Huang, H., et al., 2011. Gadolinium-induced oxidative stress triggers endoplasmic reticulum stress in rat cortical neurons. J. Neurochem. 117, 38–47.
Yeghicheyan, D., Aubert, D., Bouhnik-Le Coz, M., et al., 2019. A new interlaboratory characterisation of silicon, rare earth elements and twenty-two other trace element concentrations in the natural river water certified reference material SLRS-6 (NRC-CNRC). Geostand. Geoanal. Res. 43, 475–496.
Zhou, Z., Lu, Z., 2013. Gadolinium-based contrast agents for magnetic resonance cancer imaging. Wiley Interdiscip Rev Nanomedicine Nanobiotechnology 5, 1–18.